The Influence of Fluoroquinolone Drugs on the Bacterial Growth of *S. epidermidis* Utilizing the Unique Potential of Vibrational Spectroscopy

U. Neugebauer,[†] U. Schmid,[‡] K. Baumann,[‡] W. Ziebuhr,[§] S. Kozitskaya,[§] U. Holzgrabe,[||] M. Schmitt,[†] and J. Popp*[,†,+]

Institut für Physikalische Chemie, Friedrich-Schiller-Universität Jena, Helmholtzweg 4, Jena, 07743, Germany, Institute of Photonic Technology e.V., Albert-Einstein-Strasse 9, 07745 Jena, Germany, Institut für Pharmazeutische Chemie, TU Braunschweig, Beethovenstrasse 55, 38106 Braunschweig, Germany, Institut für Pharmazie und Lebensmittelchemie, Universität Würzburg, Am Hubland, 97074 Würzburg, Germany, and Institut für Molekulare Infektionsbiologie, Röntgenring 11, 97070 Würzburg, Germany

Received: November 26, 2006; In Final Form: January 22, 2007

Increasing resistance of many antibiotics has made the design of new drugs necessary. To assist a target-oriented search for new structures and for the elucidation of the mode of action of existing drugs, powerful analytical techniques are required. In this work, vibrational spectroscopy is used to shed more light on the as-yet elusive interaction of gyrase inhibitors of the fluoroquinolone type with their biological target inside the Gram-positive bacterium *Staphylococcus epidermidis* by investigating whole-cell changes that occur as a result of the presence of the drug moxifloxacin. IR absorption and Raman spectra with excitation off resonance ($\lambda_{exc} = 532$ nm) and in resonance with the biological targets DNA and the aromatic amino acids of gyrase ($\lambda_{exc} = 244$ nm) were recorded for unperturbed bacteria and bacteria in varying drug concentrations (0.08, 0.16, 0.27, and 0.62 μg moxifloxacin/mL bacterial culture). The spectral changes caused by the action of the drug were analyzed with the help of statistical methods, such as hierarchical cluster analysis (HCA), principal component analysis (PCA), and Fisher's linear discriminant analysis (LDA) combined with variable selection. The wavenumbers mostly affected by the action of the drug could be assigned to protein and DNA moieties, supporting the proposed mechanisms of a tertiary complex of the fluoroquinolone, the enzyme gyrase, and DNA.

Introduction

Fluoroquinolone drugs are important antibiotics. Since their discovery in the early 1960s, the basic structure of the quinolones was modified to increase their antibacterial spectrum and potency, as well as to improve their bioavailability making the quinolones useful agents for the treatment of urinary, systemic, and respiratory tract infections. The target of the fluoroquinolones is the bacterial enzyme gyrase. This essential enzyme catalyzes the introduction of negative supercoils into the DNA and is therefore responsible for the maintenance of the DNA topology within the bacterial cell. By binding to the gyrase−DNA complex, the quinolones block the transcription, the DNA replication, and storage, which results in cell death.[1] The release of broken DNA ends has been reported to accompany the quinolone action.[2] Currently, there is no definitive model for the detailed interaction of the quinolones with the gyrase−DNA complex, although mutation experiments localized the interaction area within the N-terminal domain of the GyrA subunit close to the Tyr^{122}, which is involved in the cleavage of the DNA double strands.[3] Also, parts of the GyrB subunit may be involved in stabilization the ternary complex of gyrase, DNA, and quinolone.[1,4] Shen et al. proposed a model for this ternary complex,[5] which was later modified by Morrissey et al.[6] But still the molecular details of the interaction of the fluoroquinolones with DNA and gyrase remain largely conjectural.[2] Continued study of gyrase and its inhibitors at the molecular level is necessary to understand the action of existing drugs and to provide the knowledge base to enable the understanding of the action of emerging compounds.

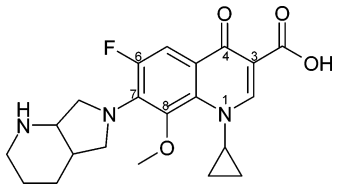

Figure 1. Structure of moxifloxacin (Moxi).

Moxifloxacin (Figure 1) is one of the newer fluoroquinolone drugs which reached the (U.K.) market in 2000 as a powerful respiratory agent. The addition of an azabicyclo group in position 7 improves the activity against Gram-positive bacteria and also brings a marked lipophilicity and half-lives of more than 10 h.[7] Moxifloxacin retains activity against many staphylococcal isolates that developed resistance to the older fluoroquinolone drug ciprofloxacin.[8] This testifies to the recognized fact in pharmaceutical and medical research that the only way to overcome the threat of growing resistances is to continuously develop new drugs.[9] In order to facilitate target-oriented research, new techniques that provide a fast and reliable insight into the mode of action of antibiotics are in high demand.

During the last years, vibrational spectroscopic methods, such as IR absorption and Raman spectroscopy, have successfully

* Corresponding author. E-mail: juergen.popp@uni-jena.de. Phone: +49-3641-948320. Fax: +49-3641-948302.
[†] Friedrich-Schiller-Universität Jena.
[‡] TU Braunschweig.
[§] Institut für Molekulare Infektionsbiologie.
[||] Universität Würzburg.
[+] Institute of Photonic Technology e.V.

10.1021/jp0678397 CCC: $37.00
Published on Web 03/27/2007

proven to have a high potential for studying biological and biomedical problems.[10] Information-rich spectra can be obtained in a rapid and noninvasive manner, making it possible to investigate structure and interactions of biomolecules in their natural environment. This was used so far, for instance, for the investigation of DNA structures,[11−13] complexation of DNA with ions,[14] structures of small peptides,[15] and proteins,[16] as well as protein-DNA binding,[17] drug−protein binding,[18] and drug−DNA[19,20] interactions. Special vibrational spectroscopic techniques allow focusing on selected traits of interest. UV resonance Raman spectroscopy, for example, enables the selective enhancement of the nucleic acid bases,[21−23] aromatic amino acids, or protein backbone vibrations, depending on the chosen excitation wavelength. Extensive UV resonance Raman studies have been performed to analyze protein and peptide secondary structure.[24−30]

But vibrational spectroscopy is also suited to probe biomolecules incorporated in more complex systems such as bacteriophages.[31,32] Highly specific and multidimensional spectral signatures are obtained from whole bacterial cells and fungi.[33−36] In addition resonance Raman spectroscopy as a marker-free technique bears high potential for clinical diagnostics and for controlling food quality.

The assignment of vibrational bands to specific functional groups, cellular compounds, or substructures in the complex bacterial spectrum allows the characterization of growth dependent phenomena,[37] culture conditions,[38−40] the influence of exposed pollutants,[41] and specific cell-drug interactions[42,43] by means of vibrational spectroscopy.

The extraction of significant and characteristic information from large data sets and the visualization of subtle differences in the spectra often necessitate the use of multivariate analysis methods such as principal component, discriminant analysis, and hierarchical cluster analysis.[44] For instance, with the help of classification techniques, it is possible to rapidly and accurately identify and classify very diverse microbial species and whole bacterial cells based on their vibrational spectra.[45−50] For classification tasks, the entire spectral information can be used. However, certain spectral regions may be irrelevant for the problem under study. Selecting a few wavenumbers which perform particularly well for classifying the data into relevant categories (i.e., bacteria treated/untreated with antibiotics) can highlight potentially important structural features and structural changes in the system under study.

The goal of this work is to use different vibrational spectroscopic techniques to gain a deeper insight into the mechanism of antibiotic action. IR absorption and micro-Raman spectroscopy with excitation at 532 nm, as well as UV resonance Raman spectroscopy with excitation at 244 nm, are applied as optical analytical tools to investigate the effect of the fluoroquinolone drug moxifloxacin on *Staphylococcus epidermidis* as an example of Gram positive bacteria. Spectra are recorded of unperturbed bacteria and of bacteria that experienced varying antibiotic concentrations. With the help of statistical methods, the spectral changes due to the action of the drug are pointed out and assigned to biological features within the cell. That way, the actual model for the mode of action of the fluoroquinolone drugs can be supported, demonstrating once again the power of vibrational spectroscopy for biomedical and pharmaceutical problems.

Experimental

S. epidermidis ATCC 35984 was grown in a batch culture in casein−peptone−soy−meal−peptone (CASO, Merck, Germany) broth at 37 °C while shaking. At the beginning of the exponential growth phase, moxifloxacin was added to the bacterial culture so that final moxifloxacin concentrations of 0.08, 0.16, 0.27, and 0.62 μg/mL were obtained in the cultivation flasks. The change of biomass with time was correlated to the vis-absorption of the bacterial suspension at 630 nm using a Spekol 1100 UV/vis spectrometer (Carl Zeiss Technology, Germany). To record the IR absorption, micro-Raman, and UV resonance Raman spectra, bacterial cells from different aliquots were washed with distilled water and placed on KRS5, CaF_2, and quartz plate, respectively, to form a homogeneous film. Eight different replicates from two different cultures have been investigated for each concentration with each spectroscopic technique.

The minimal inhibition concentration (MIC) of moxifloxacin on *S. epidermidis* ATCC 35984 was determined by drug dilution series to be <0.06 μg/mL.

IR absorption spectra were recorded on a Bruker IFS66 spectrometer with 4 cm^{-1} resolution. For each FT−IR spectrum, 128 interferograms were coadded and averaged. A DTGS (doped triglycerinsulfate) detector was used.

Micro-Raman spectra were obtained with an excitation wavelength of 532 nm from a frequency doubled Nd:YAG laser (Coherent Compass) on an invers LabRam HR spectrometer with a focal length of 800 mm (Jobin Yvon, Horiba). A Leica PLFluoar 100x microscope objective focused the laser light onto the sample with a spot size of approximately 1 μm having a laser power of approx. 10 mW incident on the sample. The 180° back-scattered Raman signal was detected with a CCD camera (1024 × 512 pixels). The integration time was 8s.

UV resonance Raman (UV RR) spectra were taken using a HR micro-Raman setup (HR800, Jobin-Yvon, Horiba). As excitation wavelength the 244 nm-line from a frequency doubled argon-ion laser (Innova 300, MotoFreD, Coherent Inc.) was applied delivering 1.1 mW at the sample. The signal was recorded with acquisition times of 120 s by a liquid N_2 cooled CCD camera. In order to avoid photodegradation, the sample was rotated so that always fresh cells were exposed to the laser beam.

The spectral data were evaluated in the spectral region between 1900 and 600 cm^{-1}. To remove the background drift in the micro-Raman spectra, the first derivative of the spectra was calculated using OPUS software (Bruker Optik GmbH). All spectra (IR, Raman) have been vector normalized before subjecting to hierarchical cluster analysis (HCA). The spectral distances were calculated by standard method (IR, 532 nm Raman data) or factorization method (UV RR data), and the clusters were prepared following Ward's technique. OPUS software (Bruker Optik GmbH) has been applied for these calculations.

Principal component analysis (PCA) was performed with the program "Unscrambler" (CAMO Process AS, Version 9.2) and used to reduce the dimensionality of the spectral data. The spectra were centered, and the model was calculated with complete cross validation. The spectra are displayed in a new coordinate system spanned by orthogonal principal components. The first-principal component is positioned along the direction of maximum variance within the data set. It was found that the bacterial spectra arrange within this new coordinate system along the first principal component (PC1) according to the added drug concentration. Therefore, the loadings for PC1 were used to identify the wavenumbers that contribute most to the spectral variances.

Wavenumbers with high importance for the discrimination of the spectra can be found with the help of a data-driven

variable selection procedure; that is, each wavenumber represents an independent variable in the classification problem. The entire data set was split 100 times into a training set (63%) and a test set (37%). Reverse elimination tabu search (REM-TS) coupled to Fisher's discriminant analysis was operated on the training set to search for highly discriminatory variables[51] and to classify the data based on the tentatively selected variable subsets. The stage-wise search of REM-TS was terminated when either six variables were included in the model or when the classification error could not be decreased by more than 3% in two consecutive iterations. The classification error was assessed by leave-multiple-out cross-validation (LMO-CV) as objective function with 50 different splits of the training data set into a construction set (75%) and a validation set (25%).[52]

The actual test set predictivity (external assessment of the classification performance) was computed such as in "bootstrap aggregating" (bagging).[53,54] In bagging, multiple models (here 100) are entertained in parallel. These models are obtained by drawing random samples out of a given dataset generating splits into training set and test set. Next, a model for each training set is computed, and on this basis, the class membership of the test set spectra is predicted. The final class assignment for a particular spectrum is based on the major vote of all models, where this spectrum was part of the test set, i.e., on average 37 models because each spectrum has approximately 37% probability to be part of the test set.[55] The classification performance is specified as the percentage of correctly assigned spectra. The occurrence of every variable in the 100 best variable subsets was calculated to assess the relevance of the wavenumbers and consequently changes of cellular components depending on interactions with different moxifloxacin concentrations.

Unlike for calculating the HCA, the background correction was not performed by using the first derivative of the spectrum but, rather, by robust curve-fitting. Variable selection with the first derivative is expected to be disadvantageous, as the spectral peaks are displaced in relation to the raw spectra, and information about the peak intensities is lost since peak maxima in the raw data represent zero crossing in the first derivative spectra. Therefore, baseline subtraction was done prior to variable selection by fitting a straight line to the baseline of the spectra using half-quadratic minimization.[56]

Due to the huge number of possible six variable models (combinatorial explosion), many can lead to equally good solutions. To improve interpretability of the models, only those regions of wavenumbers that can be assigned to spectral signals of cellular components were considered for the search (for the IR absorption spectra: 1742, 1695−1675, 1654, 1639, 1548, 1452, 1396, 1300−1240, 1239, 1085, and 720 cm^{-1}; for the micro-Raman spectra: 1660, 1614−1607, 1575, 1450, 1370−1375, 1337, 1314, 1242−1240, 1128, 1092, 1001, 899, 855, 782, 731, 723, 663, 642, and 621 cm^{-1}, and for the UV resonance Raman spectra: 1639, 1609, 1567, 1521, 1475, 1359, 1324, 1307, 1229, and 1168 cm^{-1}). Each central wavenumber and approximately ten neighboring wavenumbers were boxaveraged and constitute one spectral region. The programs for variable selection were written and validated in-house for Matlab (The Mathworks, Inc.).

Results and Discussion

The minimal inhibition concentration (MIC) of moxifloxacin on *S. epidermidis* ATCC 35984 was determined to be less than 0.06 μg/mL. This value is in good agreement with the MICs of moxifloxacin on other staphylococcus strains, as reported in the literature.[7] When the drug is applied, target peak serum concentrations of 2.5 μg/mL in the body have been reported.[57] We chose four different drug concentrations within this pharmaceutical relevant range to study the influence of moxifloxacin on bacteria in order to learn more about the mode of action of this fluoroquinolone drug.

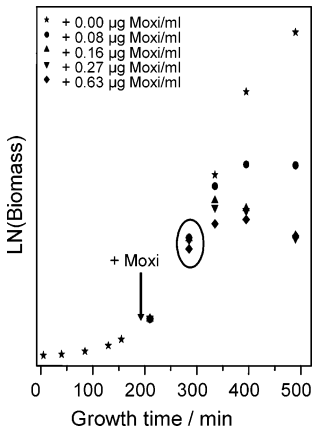

Figure 2. Growth curves of *S. epidermidis* ATCC 35984 under batch conditions (CASO, 37 °C) in the semilogarithmic representation for bacterial cultures without (★) and with the addition of different moxifloxacin concentration (● 0.8 μg/mL, ▲ 0.16 μg/mL, ▼ 0.27 μg/mL, and ♦ 0.63 μg/mL). An arrow marks the time of the addition of the drug and the ellipse highlights the time at which the following vibrational spectra have been recorded.

Figure 2 shows the growth curves of *S. epidermidis* ATCC 35984 under batch conditions (CASO, 37 °C) in the semilogarithmic representation for bacterial cultures without and with the addition of different moxifloxacin concentrations (0.08, 0.16, 0.27, and 0.63 μg/mL). The growth curve of the unperturbed culture features the typical growth phases: in the lag phase (<100 min), the bacteria prepare their metabolism for the upcoming growth phase, and no net-increase of biomass is observed. It follows the acceleration phase in which the growth rate increases until it reaches a constant value of $\mu = 0.789$ h^{-1} (37 °C in CASO) in the exponential growth phase (>180 min). Finally, the growth rate decreases again in the retardation phase and is zero in the stationary phase (>600 min).

At the beginning of the exponential growth phase bacteria are most susceptible to changes in their environment. Therefore, moxifloxacin was added in different concentrations to the growing bacterial culture at this time (200 min after inoculation of the culture; marked by an arrow in Figure 2). This causes a reduction of the overall biomass increase and finally results in a complete inhibition of the bacterial growth due to cell death, as can be seen in the growth curve at later growth times. The effect is more pronounced at higher moxifloxacin concentrations meaning that the extent of bacterial killing increases as drug concentrations increase. Several times after the addition of the drug, IR absorption, micro-Raman, and resonance Raman spectra were recorded of the bacteria without and with drug addition. In the following, the results are represented for a residence time of the drug of 80 min. This is enough time for the drug to diffuse into the bacterial cells, interact with its biological targets and initiate cell death. From pharmacodynamic studies of moxifloxacin, the time to kill 99.9% of *S. epidermidis* cells was determined to be between 90 and 180 min.[8]

IR Absorption Spectra. Figure 3A shows representative IR absorption spectra for the different drug concentrations after an incubation time of 80 min (280 min of total growth time). On a first view, all spectra look very similar. They are dominated by the strong amide I band at 1654 cm^{-1} [46] and the amide II band at 1547 cm^{-1}.[46] Other prominent features are the broad

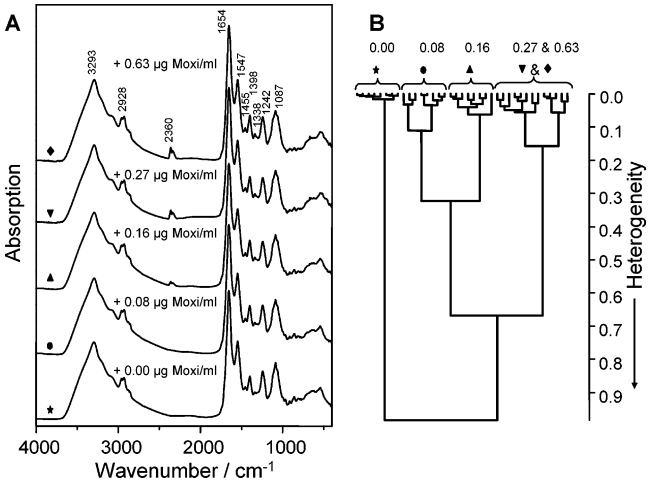

Figure 3. A: IR absorption spectra of *S. epidermidis* with different drug concentrations, recorded 80 min after drug addition (the time is marked with an ellipse in the growth curve in Figure 2). B: Hierarchical cluster analysis (HCA) of the vector normalized spectra shown in panel A). The numbers above the clusters name the added moxifloxacin concentration in μg/mL.

NH stretching band around 3291 cm^{-1} [46] and the various C−H stretches of medium intensity around 2930 cm^{-1}.[46] The C−H deformation mode is found at 1242 cm^{-1},[46] and the band at 1087 cm^{-1} [46] is due to the symmetric P═O stretching vibration. A more detailed discussion of the spectra of unperturbed *S. epidermidis* is given in reference 37.

Even though the spectra appear qualitatively very similar, quantitative differences according to the drug concentration can be found. Statistical methods help to point out the spectral traits of interest. In the hierarchical cluster analysis (HCA) shown in Figure 3B, the vector normalized spectra of bacteria without and with drug separate very well into two different clusters. The cluster of spectra of bacteria that were exposed to the antibiotics further splits according to the drug concentration. The two lowest moxifloxacin concentrations (0.08 μg/mL and 0.16 μg/mL) form each separate sub-clusters with a relatively small inner-cluster heterogeneity and are distinct from the spectra of bacteria which were treated with higher moxifloxacin concentrations (0.27 and 0.63 μg/mL). The similarity of the spectra of the two highest drug concentrations is also in good agreement with a coinciding amount of biomass present in the culture at this growth time (Figure 2). For drug concentration around the minimal inhibition concentration (the two lowest moxifloxacin concentrations), the saturation level has not been reached yet, and therefore the effect of the drug on the bacteria still increases as drug concentration increases allowing a separation of the IR spectra in distinct subclusters.

The same vibrational spectra were used to perform a principal component analysis (PCA). The scores plot of the first two principal components (PC) which describe together 88% of the explained variance is shown in Figure 4A. According to the drug concentration, the bacterial spectra arrange along the first PC, with the bacteria with no moxifloxacin and with 0.08 μg moxifloxacin/mL displaced also along the second PC. As in the HCA, no separation of the two highest moxifloxacin concentrations 0.27 and 0.63 μg/mL is achieved.

Since the first principal component correlates to the drug concentration, the loading of PC1 can be used to learn more about the wavenumbers that are associated with the largest variation due to the action of the drug (Figure 4B). The largest spectral changes occur in the wavenumber region around 1624 cm^{-1}. However, also the wavenumbers around 1710, 1660,

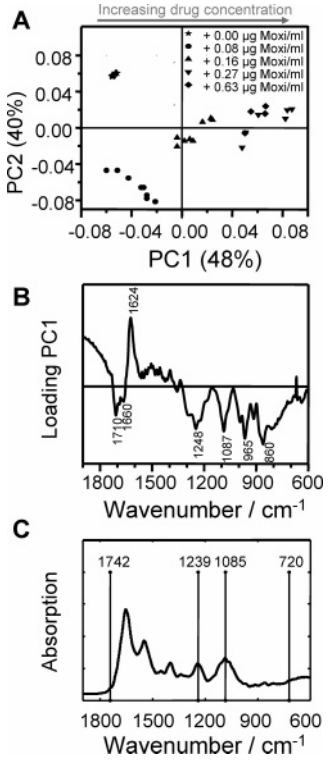

Figure 4. A: Scores plot of the first two principal components (PCs) of the IR absorption spectra of *S. epidermidis* with different drug concentrations, recorded 80 min after drug addition. B: Loading plot for the first-principal component (from A). C: Important wavenumbers determined by variable selection (REM-TS and LDA) plotted into an IR absorption spectrum of *S. epidermidis* grown in the presence of 0.16 μg/mL moxifloxacin, recorded 80 min after drug addition.

1248, 1087, 965, and 860 cm^{-1} contribute with markedly weight to PC1 (Table 1).

As a further statistical evaluation (variable selection) method, REM-TS with LDA was employed to select the wavenumbers with high discriminative power. It turned out that a couple of variable subsets achieved extremely good classification results with LDA. As a consequence the search did not yield a definite result concerning which wavenumbers are most relevant for the discrimination. One out of many equally good variable subsets is 1742, 1239, 1085, and 720 cm^{-1} (Figure 4C). Using these variables for classification achieved an internal predictivity of 98% correctly classified spectra in LMO-CV. The external predictivity of the test set spectra obtained by major voting was 93%.

This indicates that in the interaction of moxifloxacin with its biological targets and the subsequent reactions mainly changes at the DNA (symmetric and asymmetric P═O stretch in the DNA backbone), but also in protein (amide III and amide I) are involved. The contributions of the asymmetric and symmetric PO_2^- stretching vibration at 1248 and 1087 cm^{-1}, respectively, to the loading of PC1 and the selection of those wavenumbers by the tabu search method indicate structural changes in the DNA backbone, which might be a reorientation of the phosphate groups due to DNA interactions. The negative correlation of this wavenumbers in the PCA suggests a decrease of phosphate binding, which is in good agreement with the observation of DNA fragments after the incubation with fluoroquinolone drugs reported in earlier studies.[2]

Furthermore, the principal component analysis reveals a positive correlation of the wavenumber region around 1624 cm^{-1} to the loading of PC1 which indicates an increase of intermo-

TABLE 1: Assignment of the Wavenumbers Showing the Highest Discriminative Power for the Spectra (IR Absorption, Micro-Raman, and UV Resonance Raman) of Bacteria Experiencing Different Antibiotic Concentrations as Determined by Means of PCA and REM-TS/LDA, Respectively[a]

experimenal method	IR absorption			micro-Raman (λ_{exc} = 532 nm)			UV RR (λ_{exc} = 244 nm)		
evaluation method	PCA (PC1)	REM-TS/ LDA	assignment	PCA (PC1)	REM-TS/ LDA	assignment	PCA (PC1)	REM-TS/ LDA	assignment
characteristic wavenumbers in cm^{-1}		1742	C═O stretching in saturate esters[46]						
	1710								
	1660		amide I (α-helix and β-sheet)[46]	1660		amide I (C═O stretch, NH_2 bending, C═N stretch)[39,46], C═C stretch (lipids)[64]	1650		amide I
								1639	T [44]
	1624		intermolecular aggregated β-sheet of denatured protein[58]						
							1601	1609	Tyr + Trp [44]
				1581		nucleic acids (G+A ring stretch)[46]	1570		G + A [44]
							1477	1475	G + A [44]
				1462	1450	CH_2 def scissoring[39,46,59,60]			
					1314	CH def[39]			
								1307	A + G + Tyr [44]
				1298		G, CH def (protein)[64]			
				1263		amide III[39,46]			
	1248	1239	amide III; P═O str (asym) of PO_2^- (phosphodiester)[46]						
					1242	stacking-sensitive marker of dT[62]			
								1229	G + A + U[44]
				1123		C-N and CC str[39,46], ═C C═ (unsat. fatty acids in lipids)[35]			
	1087	1085	P═O stretch (sym) of PO_2^- [34], aliphatic esters[65]	1088		CC skeletal, C-O-C asym stretch in aliphatic esters, glycosidic link[46]			
	965								
	860								
					782	CC stretch ring breathing (cytosine, uracil)[39,46,59,60]			
		720	C-H rocking of CH_2[46]	741		DNA components (stacking-sensitive marker of dA[62] or dT[39,62]			

[a] The spectra were recorded after a growth time of 335 min, which is 80 min after the addition of the drug. Abbreviations: A: adenine, C: cytosine, G: guanine, T: thymine, U: uracil, Tyr: tyrosine, Trp: tryptophan, asym: asymmetric, sym: symmetric, stretch: stretching vibration, def: deformation vibration.

lecular aggregated β-sheet as they are found in denatured protein.[58] The concomitant negative correlation of PC1 with a broad region around 1660 cm^{-1} marks the decrease of ordered α-helical and β-sheet structures. This can be a consequence of the interaction of the drug with the proteins (gyrase). However, from the experiments above it is not completely clear whether the observed changes in protein structure are only due to the direct interaction of moxifloxacin with the proteins, or also contain contributions from structural changes caused by successive reactions (cell death).

Micro-Raman Spectra with Excitation at 532 nm. Figure 5 shows the micro-Raman spectra of the bacteria with and without drug addition in a spectral region between 1900 and 600 cm^{-1}. As for the IR spectra, no significant differences are visible on first sight and make a statistical analysis necessary. Due to different selection rules, different vibrational bands are prominent in the Raman spectra compared to the IR spectra. Prominent vibrational bands in the micro-Raman spectrum which can be assigned to protein contributions are the amide I band around 1660 cm^{-1},[39,46] the amide III band in the spectral region between 1220 and 1300 cm^{-1},[39,46] and the aromatic ring stretching mode of phenylalanine around 1000 cm^{-1}.[46] The vibrational bands at 1450 and 1333 cm^{-1} are assigned to CH_2 and CH deformation modes, respectively.[39,46,59,60] Nucleic acid vibrations are present in the Raman spectrum with the guanine and adenine ring stretch at 1575 cm^{-1}.[46]

In order to keep the influence of the fluorescence background low, the first derivative of the Raman spectra was used for the hierarchical cluster analysis (HCA) shown in Figure 5B. As for the IR spectra, the HCA allows a clear discrimination between the spectra of untreated bacteria and the spectra of bacteria that have been exposed to moxifloxacin. The bacterial spectra of different drug concentration form individual subclusters within the moxifloxacin cluster, but the inner-class variance is quite high. This relatively high inner-class variance of the micro-Raman spectra compared to the IR absorption spectra can be

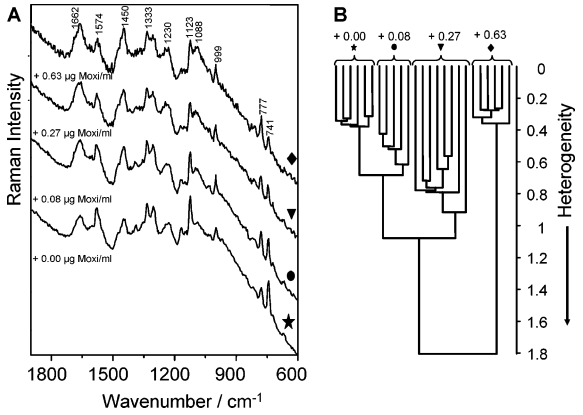

Figure 5. A: Micro-Raman spectra with excitation at 532 nm of *S. epidermidis* with different drug concentrations, recorded 80 min after drug addition. B: Hierarchical cluster analysis (HCA) of the first derivative from the spectra shown in panel A**).** The numbers above the clusters name the added moxifloxacin concentration in μg/mL.

explained with different amount of bacterial cells probed with one scan. For the IR absorption spectra, the averaged signal results from 10^6 to 10^8 individual cells, while only about 30 cells contribute to the micro-Raman spectrum.[61]

For performing the principal component analysis (PCA) and the REM-TS/LDA the markedly fluorescence background of the Raman spectra was removed by baseline correction rather than by using the first derivative, because information about exact peak position and intensity are desirable when assigning the loadings for the principal components. The scores plot of the first two principal components of the PCA is shown in Figure 6A. No clean separation of the individual antibiotic concentrations is achieved when using only two PCs. However, as for the IR spectra, it is again the first principal component that correlates with the addition of the drug. Figure 6B indicates strong contributions of the wavenumbers due to DNA to the loading of PC1. The strong positive loadings at 1581, 1123, and 741 cm^{-1} can be assigned to ring stretching vibrations in guanine and adenine,[46] to C−N and C−C stretching vibrations,[39,46] and to stacking sensitive vibrations of adenosine and thymidine,[39,62] respectively. Further DNA contributions are present with the band at 1088 cm^{-1} from glycosidic linkages and symmetric PO_2^- stretching vibrations of the DNA backbone. Changes in the protein structure are indicated by the loadings of the amide I band around 1660 cm^{-1} and the amide III band around 1263 cm^{-1}. The negative correlation of these bands denotes an increase of random coil structure[63] upon the addition of the drug. This is in good agreement with the results from the IR absorption measurements. The loadings around 1462 cm^{-1} are due to molecular changes affecting CH-deformation modes.

The importance of the wavenumbers associated with changes in DNA for the differentiation of the micro-Raman spectra of *S. epidermidis* cells which experienced varying antibiotic concentrations is also revealed by REM-TS coupled to LDA (Table 1). Using this variable selection process resulted in a variable subset with the wavenumbers 1242 and 782 cm^{-1} as well as 1450 and 1314 cm^{-1} (Figure 6C). The wavenumber at 782 cm^{-1} can be assigned to the ring-breathing mode in cytosine (and also uracil),[39,46,59,60] the wavenumber 1242 cm^{-1} can be assigned to stacking sensitive vibrations of thymine. The wavenumbers at 1314 and 1450 cm^{-1} could be due to CH vibrations of the sugar moiety of the DNA (Figure 6C, Table 1). However, a definite ranking concerning the importance of the wavenumbers could not be obtained as the classification by

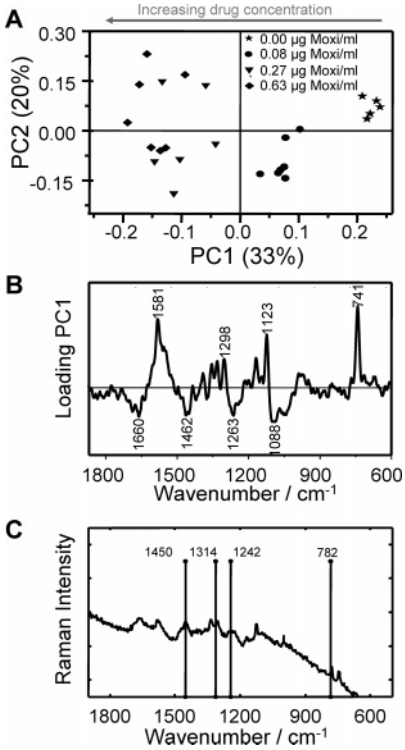

Figure 6. A: Scores plot of the first two principal components (PCs) when using baseline corrected micro-Raman spectra with excitation at 532 nm of *S. epidermidis* with different drug concentrations, recorded 80 min after drug addition. B: Loading plot for the first principal component (from A). C: Important wavenumbers determined by variable selection (REM-TS and LDA) plotted into a micro-Raman spectrum of *S. epidermidis* grown in the presence of 0.08 μg/mL moxifloxacin, recorded 80 min after drug addition.

LDA showed an equally good performance for many subsets. The chosen variable subset (1242 and 782 cm^{-1} as well as 1450 and 1314 cm^{-1}, Figure 6C) showed very good recognition rates and 100% of the spectra could be classified correctly in LMO-CV (internal predictivity). The test set recognition rate obtained by major voting was 96% (external predictivity).

The selected wavenumbers that experience changes upon addition of moxifloxacin support the proposed mechanism of action of the fluoroquinolone drugs. The drug, in our case moxifloxacin, interacts simultaneously with the DNA double strand while binding to the protein gyrase. Therefore, vibrational bands due to DNA and protein should be affected by the addition of the drug. However, it should be noted that 80 min after drug addition further reactions might have occurred. Contributions of the drug itself to the Raman spectra of the bacteria can be neglected, since moxifloxacin is so effective against staphylococci (MIC < 0.06 μg/mL) that only low antibiotic concentrations are required in the cultivation flasks to kill the bacteria. Aqueous solutions of moxifloxacin at concentrations below 1.5 μg/μl did not result in any Raman spectra with noticeable signal. Therefore, the direct influence of the pure presence of the drug on the variance of the bacterial spectra with different drug concentration can be neglected. The observed variances within the spectra must be due to changes within the bacteria that are caused by the action of the drug.

UV Resonance Raman Spectra with Excitation at 244 nm. In the proposed mechanisms of action of the fluoroquinolone drugs, the DNA and the enzyme gyrase are involved. It was shown above that changes in the protein and DNA moieties of the bacterium can indeed be found in the spectra upon drug addition. UV resonance Raman spectroscopy with an excitation

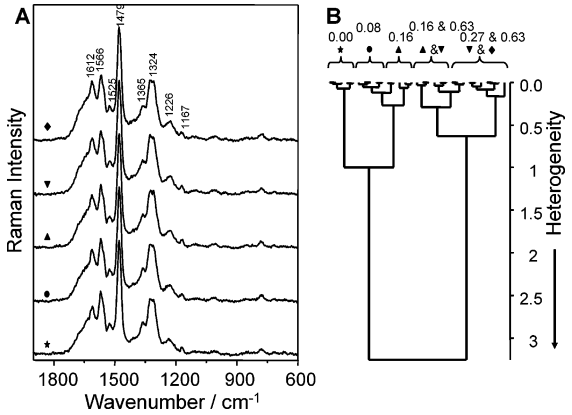

Figure 7. A: UV resonance Raman spectra with excitation at 244 nm of *S. epidermidis* with different drug concentrations recorded 80 min after drug addition. B: Hierarchical cluster analysis (HCA) of the vector normalized spectra shown in panel A). The numbers above the clusters name the added moxifloxacin concentration in μg/mL.

wavelength of 244 nm allows especially focusing on the purine and pyrimidine bases of the nucleic acids and on the aromatic amino acids in the proteins.

The UV resonance Raman spectra of the bacteria without and with different drug concentration shown in Figure 7A are dominated by contributions from the purine and to a lesser extend the pyrimidine bases of the nucleic acids. Guanine and adenine moieties account for the vibrational bands at 1479 and 1566 cm^{-1}. Cytosine is responsible for the weak band at 1525 cm^{-1} and thymine and adenine contribute to the band at 1365 cm^{-1}. Amino acid vibrations are present with the aromatic amino acids tyrosine and tryptophan which show up at 1612 and 1167 cm^{-1}. The band at 1324 cm^{-1} results from vibrations in the adenine, guanine and tyrosine moieties.

Unlike for the IR and non-resonance Raman spectra, the hierarchical cluster analysis of the UV resonance Raman spectra (Figure 7B) reveals a high heterogeneity of the bacteria which were exposed to high moxifloxacin concentrations (0.63 and 0.27 μg/mL) and those which experienced no or a lower moxifloxacin concentration. Within the low-moxifloxacin concentration cluster, the bacterial spectra of the reference culture (no drug) are very well separated from those which were treated with the drug. The two lowest drug concentrations (0.08 and 0.16 μg/mL) form subclusters which contain also one spectrum of the other drug concentration. Within the cluster of the high moxifloxacin concentrations, no clear subcluster formation according to the concentration is observed. This suggests that the changes within the bacteria due to the drug are the same for the two highest drug concentrations of 0.26 and 0.63 μg/mL, as was already observed for the IR absorption spectra. Those concentrations are well above the MIC of moxifloxacin for *S. epidermidis*, while 0.08 and 0.16 μg/mL are on the order of magnitude of the MIC (0.06 μg moxifloxacin/mL bacterial culture).

The scores plot of the first two principal components of the PCA shown in Figure 8A features the same classification pattern as the HCA: the spectra of the bacteria without drug and with low drug concentration are found on the positive side of the first principal component while the spectra of bacteria with high drug concentrations form a mixed cluster on the negative end of PC1. Even though no clear, well-separated clusters are formed, the variation in the spectra due to the effect of the drug can be correlated with the first principal component. In particular, the vibrational bands around 1650 and 1600 cm^{-1} (negatively correlated) as well as the bands at 1570

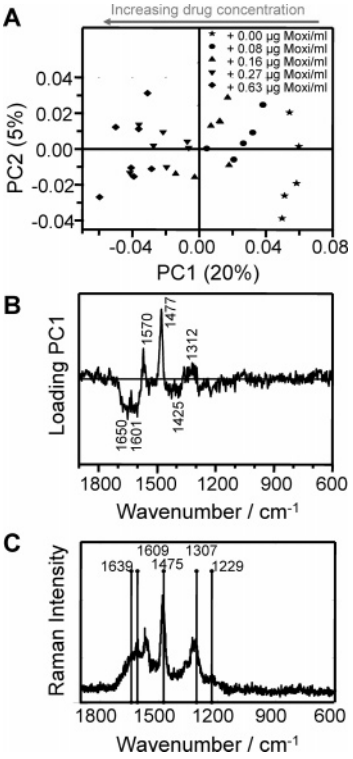

Figure 8. A: Scores plot of the first two principal components (PCs) of the UV resonance Raman spectra with excitation at 244 nm of *S. epidermidis* with different drug concentrations recorded 80 min after drug addition. B: Loading plot for the first principal component (from panel A). C: Important wavenumbers determined by variable selection (REM-TS and LDA) plotted into a UV resonance Raman spectrum of *S. epidermidis* grown in the presence of 0.08 μg/mL moxifloxacin, recorded 80 min after drug addition.

and 1477 cm^{-1} (positively correlated) contribute to this principal component as can be seen from the loading plot in Figure 8B.

The importance of the wavenumbers at 1609 and 1475 cm^{-1} for the classification of the data is also reproduced by subset selection by REM-TS and LDA. The wavenumbers 1609 and 1229 cm^{-1} were selected most often during the search procedure with an occurrence of >80 out of the 100 runs with different splits into training set and test set. Moreover, the spectral regions at 1639, 1475, and 1307 cm^{-1} were selected more than 30 times out of the 100 runs (Figure 8C). A combination of the five strongest regions of wavenumbers with an occurrence of more than 30 times out of the 100 runs achieved a recognition rate of 74% by LMO-CV and LDA (internal predictivity). By major voting 69% of the spectra were classified correctly (external predictivity). This relative low internal predictivity is in line with the mixed clusters in the HCA and PCA. Nevertheless, the selection of the relevant wavenumbers is quite clear and supports the proposed mechanism by putting special focus on the DNA (especially adenine and guanine) and protein moieties (especially amide I and the aromatic amino acids tryptophan and tyrosine). It should be noted that the binding of the DNA double strand to the gyrase occurs via an ester linkage to tyrosine Tyr^{122} of the enzyme. The presence of different moxifloxacin concentrations within the bacterial cells does not seem to influence the classification since the wavenumbers of the two strongest vibrational bands of the resonance Raman spectrum of moxifloxacin (1619 and 1548 cm^{-1}) have neither been selected by REM-TS/LDA nor showed markedly contributions to the loadings of PC1 from the PCA.

Summary and Conclusion

IR absorption, micro-Raman, and UV resonance Raman spectra were recorded to monitor the effect of the gyrase-inhibitor moxifloxacin on *Staphylococcus epidermidis*. With the help of multivariate statistical methods, it was possible to distinguish between bacterial cells that grew under unperturbed conditions and those cells that were exposed to different concentrations of the antibiotics. It was even possible to classify the bacterial spectra according to the added drug concentrations. At concentrations around the MIC (0.08 and 0.16 μg/mL), the extent of the effect of the drug on the bacteria seems to increase as the moxifloxacin concentration increases. At drug concentrations well above the MIC (0.27 and 0.63 μg/mL), the vibrational spectra could hardly be distinguished and are mixed in the statistical analysis. This suggests that the same biological processes occur within the cell upon drug addition when the drug concentration is well above the MIC (saturation effect). This assumption is in agreement with the very similar biomass concentrations of the bacterial suspensions of those two antibiotic concentrations at the sampling time as can be seen in the growth curve (Figure 2). The wavenumbers that are responsible for the classification of the spectra could be determined by the data-driven selection procedure of reverse elimination tabu search coupled to Fisher's discriminant analysis (REM-TS/LDA). Furthermore, it was possible to find a correlation between the first principal component and the drug concentration in the bacterial suspension when using principal component analysis to identify the wavenumbers that experience the largest variations upon drug addition. Even though the different spectroscopic techniques focus on different aspects of the cells, they all agree that the drug causes changes within the cell being mainly associated with changes in the DNA and protein moieties (Table 1). This supports the proposed mechanism of the action of the drugs of the fluroquinolone type: they attack the gyrase-DNA complex which causes subsequent reactions that affect the DNA and protein structure.

This work clearly demonstrates that vibrational spectroscopy, namely, IR absorption, micro-Raman spectroscopy with excitation in the visible, and UV resonance Raman spectroscopy, can be used in combination with advanced statistical data analysis to study the influence of drugs on microorganisms. Furthermore, resonance Raman spectroscopy allows the selective enhancement of the Raman signals of certain chromophoric segments within the bacterial cell. Valuable information corresponding to the molecular interactions of the drug and its following metabolic changes can be extracted from the multidimensional spectra by means of multivariate statistical methods. These techniques bear high potential for the characterization of the mode of action of various drugs in a fast and reliable manner, and therefore could assist on the way to develop new and powerful drugs.

Acknowledgment. We acknowledge the support by the Deutsche Forschungsgemeinschaft (Sonderforschungsbereich SFB630, Teilprojekte A1, B5, C1, and C5).

References and Notes

(1) Barnard, F. M.; Maxwell, A. *Antimicrob. Agents Chemother.* **2001**, *45*, 1994.

(2) Mitscher, L. A. *Chem. Rev.* **2005**, *105*, 559.

(3) Heddle, J. G.; Barnard, F. M.; Wentzell, L. M.; Maxwell, A. *Nucleosides Nucleotides Nucleic Acids* **2000**, *19*, 1249.

(4) Heddle, J.; Maxwell, A. *Antimicrob. Agents Chemother.* **2002**, *46*, 1805.

(5) Shen, L. L.; Baranowski, J.; Pernet, A. G. *Biochemistry* **1989**, *28*, 3879.

(6) Morrissey, I.; Hoshino, K.; Sato, K.; Yoshida, A.; Hayakawa, I.; Bures, M. G.; Shen, L. L. *Antimicrob. Agents Chemother.* **1996**, *40*, 1775.

(7) Andersson, M. I.; MacGowan, A. P. *J. Antimicrob. Chemother.* **2003**, *51 (Suppl. S1*), 1.

(8) Lister, P. D. *Clin. Infect. Dis.* **2001**, *32*, S33.

(9) Leeb, M. *Nature* **2004**, *431*, 892.

(10) Naumann, D. In *Encyclopedia of Analytical Chemistry*; Meyers, R. A., Ed.; John Wiley & Sons Ltd.: Chichester, U.K., 2000; p 102.

(11) Benevides, J. M.; Wang, A. H.-J.; Marel, G. A. v. d.; Boom, J. H. v.; Thomas, G. J., Jr. *Biochemistry* **1989**, *28*, 304.

(12) Braun, C. S.; Jas, G. S.; Choosakoonkriang, S.; Koe, G. S.; Smith, J. G.; Middaugh, C. R. *Biophys. J.* **2003**, *84*, 1114.

(13) Deng, H.; Bloomfield, V. A.; Benevides, J. M.; Thomas, G. J., Jr. *Biopolymers* **1999**, *50*, 656.

(14) Ahmad, R.; Arakawa, H.; Tajmir-Riahi, H. A. *Biophys. J.* **2003**, *84*, 2460.

(15) Schweitzer-Stenner, R.; Eker, F.; Huang, Q.; Griebenow, K.; Mroz, P. A.; Kozlowski, P. M. *J. Phys. Chem. B* **2002**, *106*, 4294.

(16) Serban, D.; Arcineigas, S. F.; Vorgias, C. E.; Thomas, G. J., Jr. *Protein Sci.* **2003**, *12*, 861.

(17) Wojtuszewski, K.; Mukerji, I. *Protein Sci.* **2004**, *13*, 2416.

(18) Couling, V. W.; Fischer, P.; Klenerman, D.; Huber, W. *Biophys. J.* **1998**, *75*, 1097.

(19) Lee, S. A.; Rupprecht, A.; Chen, Y. Z. *Phys. Rev. Lett.* **1998**, *80*, 2241.

(20) Manfait, M.; Alix, A. J. P.; Jeannesson, P.; Jardillier, J.-C.; Theophanides, T. *Nucleic Acids Res.* **1982**, *10*, 3803.

(21) Wu, Q.; Nelson, W. H.; Elliott, S.; Sperry, J. F.; Feld, M.; Dasari, R.; Manoharan, R. *Anal. Chem.* **2000**, *72*, 2981.

(22) Wu, Q.; Hamilton, T.; Nelson, W. H.; Elliott, S.; Sperry, J. F.; Wu, M. *Anal. Chem.* **2001**, *73*, 3432.

(23) Fodor, S. P. A.; Spiro, T. G. *J. Am. Chem. Soc.* **1986**, *108*, 3198.

(24) Asher, S. A.; Ianoul, A.; Mix, G.; Boydon, M. N.; Karnoup, A. S.; Diem, M.; Schweitzer-Stenner, R. *J. Am. Chem. Soc.* **2001**, *123*, 11775.

(25) Asher, S. A.; Mikhonin, A. V.; Bykov, S. *J. Am. Chem. Soc.* **2004**, *126*, 8433.

(26) Boydon, M. N.; Asher, S. A. *Biochemistry* **2001**, *40*, 13723.

(27) Chi, Z.; Chen, X. G.; W. Holtz, J. S.; Asher, S. A. *Biochemistry* **1998**, *37*, 2854.

(28) Couling, V. W.; Foster, N. W.; Klenerman, D. *J. Raman Spectrosc.* **1997**, *28*, 33.

(29) Lippert, J. L.; Tyminski, D.; Desmeules, P. J. *J. Am. Chem. Soc.* **1976**, *98*, 7075.

(30) Mikhonin, A. V.; Myshakina, N. S.; Bykov, S.; Asher, S. A. *J. Am. Chem. Soc.* **2005**, *127*, 7712.

(31) Wen, Z. Q.; Overman, S. A.; Bondre, P.; Thomas, G. J., Jr. *Biochemistry* **2001**, *40*, 449.

(32) Overman, S. A.; Thomas, G. J., Jr. *Biochemistry* **1999**, *38*, 4018.

(33) Rösch, P.; Harz, M.; Schmitt, M.; Peschke, K.-D.; Ronneberger, O.; Burkhardt, H.; Motzkus, H.-W.; Lankers, M.; Hofer, S.; Thiele, H.; Popp, J. *SPIE* **2006**.

(34) Maquelin, K.; Choo-Smith, L.-P.; Endtz, H. P.; Bruining, H. A.; Puppels, G. J. *J. Clin. Microbiol.* **2002**, *40*, 594.

(35) Schuster, K. C.; Reese, I.; Urlaub, E.; Gapes, J. R.; Lendl, B. *Anal. Chem.* **2000**, *72*, 5529.

(36) Rösch, P.; Harz, M.; Peschke, K.-D.; Ronneberger, O.; Burkhardt, H.; Popp, J. *Biopolymers* **2006**, *82*, 312.

(37) Neugebauer, U.; Schmid, U.; Baumann, K.; Ziebuhr, W.; Kozitskaya, S.; Deckert, V.; Schmitt, M.; Popp, J. *ChemPhysChem* **2007**, *8*, 124−137.

(38) Schuster, K. C.; Urlaub, E.; Gapes, J. R. *J. Microbiol. Methods* **2000**, *42*, 29.

(39) Maquelin, K.; Choo-Smith, L.-P.; Vreeswijk, T. v.; Endtz, H. P.; Smith, B.; Bennett, R.; Bruining, H. A.; Puppels, G. J. *Anal. Chem.* **2000**, *72*, 12.

(40) Manoharan, R.; Ghiamati, E.; Chadha, S.; Nelson, W. H.; Sperry, J. F. *Appl. Spectrosc.* **1993**, *47*, 2145.

(41) Singer, A. C.; Huang, W. E.; Helm, J.; Thompson, I. P. *J. Microbiol. Methods* **2005**, *60*, 417.

(42) Lopez-Diez, E. C.; Winder, C. L.; Ashton, L.; Currie, F.; Goodacre, R. *Anal. Chem.* **2005**, *77*, 2901.

(43) Neugebauer, U.; Schmid, U.; Baumann, K.; Holzgrabe, U.; Ziebuhr, W.; Kozitskaya, S.; Kiefer, W.; Schmitt, M.; Popp, J. *Biopolymers* **2006**, *82*, 306.

(44) Lopez-Diez, E. C.; Goodacre, R. *Anal. Chem.* **2004**, *76*, 585.

(45) Jarvis, R. M.; Goodacre, R. *FEMS Microbiol. Lett.* **2004**, *232*, 127.

(46) Maquelin, K.; Kirschner, C.; Choo-Smith, L.-P.; Braak, N. v. d.; Endtz, H. P.; Naumann, D.; Puppels, G. J. *J. Microbiol. Methods* **2002**, *51*, 255.

(47) Rösch, P.; Harz, M.; Schmitt, M.; Peschke, K.-D.; Ronneberger, O.; Burkhardt, H.; Motzkus, H.-W.; Lankers, M.; Hofer, S.; Thiele, H.; Popp, J. *Appl. Environ. Microbiol.* **2005**, *71*, 1626.

(48) Rösch, P.; Harz, M.; Krause, M.; Petry, R.; Peschke, K.-D.; Burkhardt, H.; Ronneberger, O.; Schüle, A.; Schmauz, G.; Riesenberg, R.; Wuttig, A.; Lankers, M.; Hofer, S.; Thiele, H.; Motzkus, H.-W.; Popp, J. In *Biophotonics*; Popp, J., Strehle, M., Eds.; Wiley-VCH Verlag GmbH & C. KGaA: Weinheim, Germany, 2006, p 89.

(49) Gaus, K.; Rösch, P.; Petry, R.; Peschke, K.-D.; Ronneberger, O.; Burkhardt, H.; Baumann, K.; Popp, J. *Biopolymers* **2006**, *82*, 286.

(50) Rösch, P.; Harz, M.; Peschke, K.-D.; Ronneberger, O.; Burkhardt, H.; Schüle, A.; Schmauz, G.; Lankers, M.; Hofer, S.; Thiele, H.; Motzkus, H.-W.; Popp, J. *Anal. Chem.* **2006**, *78*, 2163.

(51) Baumann, K.; Albert, H.; von Korff, M. *J. Chemom.* **2002**, *16*, 339.

(52) Baumann, K. *QSAR Combi. Sci.* **2005**, *24*, 1033.

(53) Breiman, L. *Mach. Learn.* **1996**, *24*, 123.

(54) Wolpert, D. H.; Macready, W. G. *Mach. Learn.* **1999**, *35*, 41.

(55) Dietterich, T. G. *Ensemble Methods in Machine Learning*; Springer: Berlin, 2001.

(56) Mazeta, V.; Carteret, C.; Brie, D.; Idier, J.; Humbert, B. *Chemom. Intell. Lab. Syst.* **2005**, *76*, 121.

(57) MacGowan, A. P.; Bowker, K. E.; Wootton, M.; Holt, H. A. *J. Antimicrob. Chemother.* **1999**, *44*, 761.

(58) Torrecillas, A.; Corbalan-Garcia, S.; Gomez-Fernandez, J. C. *Biochemistry* **2004**, *43*, 2332.

(59) Xie, C.; Lie, Y.-q.; Tang, W.; Newton, R. J. *J. Appl. Phys.* **2003**, *94*, 6138.

(60) Williams, A. C.; Edwards, H. G. M. *J. Raman Spectrosc.* **1994**, *25*, 673.

(61) Gaus, K. *Diplomarbeit*, Friedrich-Schiller-Universität Jena, Jena, Germany, 2005.

(62) Benevides, J. M.; Serban, D.; Thomas, G. J., Jr. *Biochemistry* **2006**, *45*, 5359.

(63) Chen, M. C.; Lord, R. C. *J. Am. Chem. Soc.* **1974**, *96*, 4750.

(64) Notingher, I.; Verrier, S.; Polak, H. S. J. M.; Hench, L. L. *Biopolymers (Biospectroscopy)* **2003**, *72*, 230.

(65) Filip, Z.; Herrmann, S.; Kubat, J. *Microbiol. Res.* **2004**, *159*, 257.